Available online at www.sciencedirect.com

ScienceDirect

Journal of Magnesium and Alloys 7 (2019) 545–554

www.elsevier.com/locate/jma

Comparison of microstructures and mechanical properties of composite extruded AZ31 sheets

Yanfu Chai[a], Yan Song[a], Bin Jiang[a,b,*], Jie Fu[a,**], Zhongtao Jiang[c], Qingshan Yang[b], Haoran Sheng[d], Guangsheng Huang[a], Dingfei Zhang[a], Fusheng Pan[a,b]

[a] *State Key Laboratory of Mechanical Transmissions, College of Materials Science and Engineering, Chongqing University, Chongqing 400044, China*
[b] *Chongqing Academy of Science and Technology, Chongqing 401123, China*
[c] *Research Institute for New Materials Technology, Chongqing University of Arts and Sciences, Chongqing 402160, China*
[d] *Shanghai Aerospace Equipment Manufactory, Shanghai 200245, China*

Received 15 May 2019; received in revised form 30 August 2019; accepted 3 September 2019
Available online 15 November 2019

Abstract

The microstructures and mechanical properties of the composite extruded AZ31/AZ31 and AZ31/4047 Al sheets were investigated and made a comparison to the conventional extruded AZ31 sheet. Owing to the introduced intense shear deformation at the interface during the composite extrusion, grain refinement and tilted texture were detected in AZ31 layers of the AZ31/AZ31 and AZ31/4047 Al sheets, while the conventional extruded AZ31 sheet exhibited a relative coarse, inhomogeneous microstructure and strong basal texture. The compression-tension yield ratio was increased gradually from the AZ31 to the AZ31/AZ31 and AZ31/4047 Al sheets. Besides, the AZ31/4047 Al sheet could successfully accomplish the whole bending forming process at room temperature, while the AZ31 and AZ31/AZ31 sheets were both bend-formed to failure with significant cracks in the outer tensile region under the identical bending parameters. Moreover, under the same bending strain, both the outward offset degree of strain neutral layer and the sheet thickening were more serious in the AZ31/4047 Al composite sheet than those of the AZ31 and AZ31/AZ31 sheets. The foremost reason was the quite wide gap of material properties between Mg alloy AZ31 layer (tensile loading in the outer region) and Al 4047 layer (compressive loading in the inner region).

Keywords: Mg alloy sheet; Composite extrusion; Tension–compression yield asymmetry; Bendability.

1. Introduction

Magnesium alloys have attracted more and more attention in many application fields, such as automotive, aerospace, aviation, and consumption electrical products, due to the advantages of low mass density, excellent castability and efficient recyclability, etc. [1–6]. Unfortunately, inherent hexagonal close-packed (HCP) crystal structured Mg alloys possess limited available numbers of activated slip systems and resulting poor ductility and unsatisfactory forming ability at room temperature [7,8]. Significant yield anisotropy has been reported for strong basal-textured Mg alloys, such as the extruded or rolled commercial AZ31 alloys, due to the different activated eases between deformation twinning and slip systems [9]. Besides, the conventional extruded AZ31 sheet featured undesirable bending performance at room temperature, in which fracture cracks tended to initiate on the surface of the outer tensile region [10].

In comparison to Mg alloys, Al alloys usually own excellent formability and corrosion resistance, whereas Mg/Al composite materials possess good combined mechanical

* Corresponding author at: State Key Laboratory of Mechanical Transmissions, College of Materials Science and Engineering, Chongqing University, Chongqing 400044, China.
** Corresponding author.
E-mail addresses: jiangbinrong@cqu.edu.cn (B. Jiang), fujie3057@cqu.edu.cn (J. Fu).

https://doi.org/10.1016/j.jma.2019.09.007

Table 1
Actual chemical composition of the Mg alloy (AZ31) and Al alloy (4047), respectively.

Nominal alloys	Composition (wt%)				
	Mg	Al	Zn	Mn	Si
Mg alloy(AZ31)	Bal.	2.777	0.634	0.213	–
Al alloy(4047)	–	Bal.	0.028	–	9.916

properties, which are difficult to be achieved by the individual constituents [11]. Correspondingly, in the recent years, many researchers have concentrated on fabricating Mg/Al composite materials to improve the room temperature mechanical properties of Mg alloys. For instance, Feng et al. [12] stated the Mg/Al composite rods have much higher tensile or compressive yield strength than that of monolithic Mg rod. Similarly, Wu et al. [13] fabricated Mg AZ31/Al 7050 laminate composites via extrusion process. They concluded that an Al fraction of 40.2% could significantly enhance the yield strength (from 155 MPa to 300 MPa), while weight increased by only 20%. Hence, Mg/Al composite material is a promising candidate to greatly extend the potential usage of Mg alloys. Compared with the conventional way of combinations (accumulative roll bonding [14], twin-roll casting [15] and continuous casting [16]), hot extrusion is always served as a simplicity and economy process to produce effectively Mg alloy sheet, and the related investigations are abundant. However, investigations concerning microstructures and mechanical properties evolution of composite Mg/Al alloy during or after co-extrusion are seldom reported, owing to complicated flowing behaviors of the two alloys in a coexisting condition during hot deformation. In the present work, composite extrusion technology was adopted to successfully fabricate Mg–3Al–Zn/Mg–3Al–Zn (AZ31/AZ31) and Mg–3Al–Zn/4047 Aluminum (AZ31/4047 Al) sheets. Subsequently, the effect of the introduced Mg/Mg, Mg/Al interfaces on the microstructure and texture evolution during hot extrusion was examined in detail. Meanwhile, a further intention of the present research was to assess the role of introduced interface and Al laminate superposition during composite extrusion on the ultimate tension-compression yield asymmetry (TCA) and bendability of sheets at room temperature.

2. Experimental procedures

The actual chemical compositions of the as-cast AZ31 Mg and 4047 Al alloys were inspected by X-ray fluorescence spectrometer (XRF-1800CCDE) and corresponding results were shown in Table 1. Subsequently, the as-cast ingots were machined into cylinder-shaped ones with 80 mm in diameter and 60 mm in height, and then were homogenized at 400 °C for 12 h prior to the extrusion. Extrusion process was carried out at 400 °C under a ram speed of 3 mm s^{-1} with an extrusion ratio of 36:1. Its specific details were illustrated in Fig. 1, the AZ31/AZ31 and AZ31/4047 Al sheets were produced successfully by composite extrusion, meanwhile, the conventional extruded AZ31 sheet was also conducted for comparison. The composite extrusion process, invented by Pan et al. [17,18], which could improve effectively the mechanical properties of AZ31 Mg alloy sheets. The core point was that the entire AZ31 ingot was divided into specific pieces prior to extrusion through wire-electrode cutting, which eventually introduced additional composite interfaces and additional shear deformation during extrusion. Details of the composite extrusion process include the following several parts: (1) one whole ingot was cut into average half along the axis direction. (2) Removed the oxide layer on the surface of blocks by using a grinding machine. (3, 4) These separate pieces were bundled as a whole cylinder ingot and then using a thick silver paper to cover these fresh surfaces.

Tensile and compressive tests were carried out by using CMT6305-300KN testing machine with a strain rate of 10^{-3} s^{-1} at room temperature. Tensile samples with a gage length of 14 mm, width of 6 mm and thickness of 2.5 mm were machined from three sheets along extrusion direction (ED). Rectangular specimens with nominal dimensions of 10 mm × 8 mm × 2.5 mm were prepared for the compressive tests. At least three samples for each condition were repeatedly tested and the resulting data were averaged. The yield strength was measured as 0.2% proof stress and the extent of yield asymmetry was described as the ratio of compressive yield stress to tensile yield stress (C/T). Specimens for V-bending tests were machined from three sheets along the ED with the dimensions of 55 mm × 12 mm × 2.5 mm. Fig. 2 presents the schematic diagrams of V-bending process for three sheets. The radius and angle of the punch were 6 mm and 90°, respectively, meanwhile the velocity of punch was set as 3 mm/min. Besides, five samples were conducted in each group to warrant the experimental precision.

The micro-structural characterization of AZ31 layer of the three extruded sheets was examined from the extrusion direction (ED)-normal direction (ND) plane by means of Optical microscopy (OM). Specimen preparation for OM observation was ground, polished and then etched with a solution of 100 ml ethanol, 10 ml water, 5 ml acetic acid and 5 g picric acid. Average grain sizes were obtained by the linear intercept method via Image-Pro Plus 6 software. In order to disclose the effect of the introduced Mg/Mg, Mg/Al interfaces on texture evolution of AZ31 layers in composite sheets, the macro-texture was evaluated by using X-ray diffraction (XRD, Rigaku D/Max 2500) with Cu Ka radiation. The condition of intermediate diffusion layer was assessed by scanning electron microscope (SEM; Tescan Vega 3 LMH) equipped with an energy-dispersive X-ray spectrometer (EDS; OXFORD INCA) system. Sample preparation for electron backscatter diffraction (EBSD) analysis consisted of metallurgical polishing and followed electro-polishing in an AC2 electrolyte, using a voltage of 20 V for ~70 s at −20 °C. EBSD measurements were taken in the ED-ND plane of three bended samples at 20 KV and a scan step of 0.6 μm for the sake of observing the offset degree of strain neutral layer intuitively.

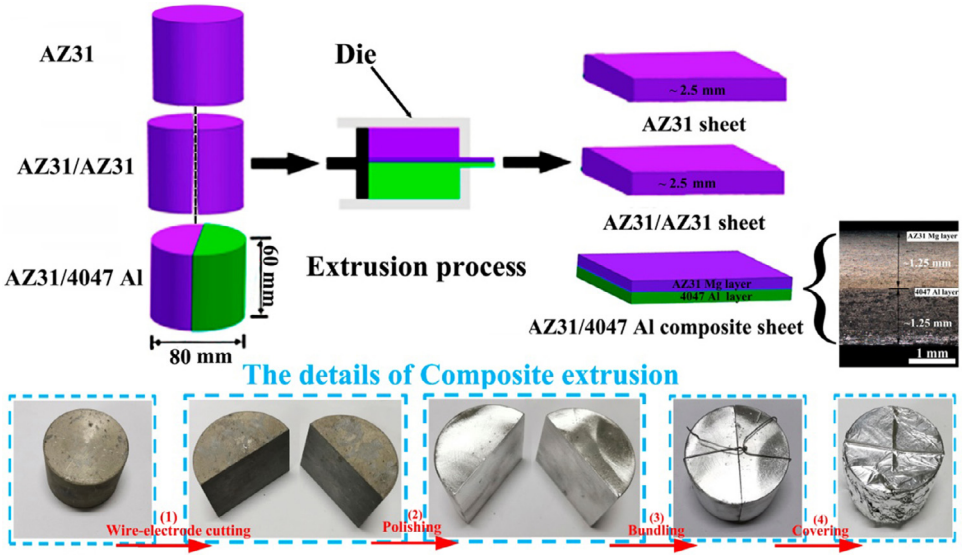

Fig. 1. Schematic diagrams of the fabrication for three sheets and the details of composite extrusion process.

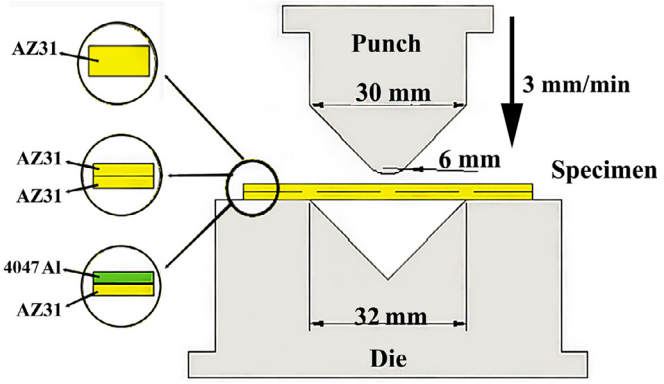

Fig. 2. Schematic diagrams of V-bend forming for three sheets.

3. Results and discussion

3.1. Simulation results

A finite element model (FEM) is employed using DEFORM-3D software to investigate and compare the effective strain evolution during the conventional and composite extrusion processes, and the related results are demonstrated in Fig. 3. Remarkably, it can be seen that an additional effective strain (marked by a black ellipse) exists at the interface of AZ31/AZ31 and AZ31/4047 Al sheets (see Fig. 3(b) and (c)), while the counterpart in AZ31 sheet is missed (see Fig. 3(a)). Moreover, it is noteworthy that the additional effective strain at the interface of AZ31/4047 Al sheet is higher than that of AZ31/AZ31 sheet. The possible reason is ascribed to the different flow behavior between AZ31 and 4047 Al alloys.

The effective strain evolutions in the top and bottom surfaces of the conventional and composite extruded AZ31 sheets are presented in Fig. 3(d)–(f). The results indicate that the effective strain distribution of the conventional extruded AZ31 sheet is almost the same on its top and bottom surfaces. In contrast, an evident effective strain gradient is formed throughout the thickness direction of the composite extruded AZ31/AZ31 and AZ31/4047 Al sheets.

3.2. The morphology of Mg/Al bonding interface and element diffusion

Fig. 4 illustrates the SEM image of diffusion reaction layer in AZ31/4047 Al composite extruded sheet. The results indicate that there are no voids and cracks between these two dissimilar metals adjacent to the transition layer. In addition, the thickness of the transition layer is approximately 3.6 μm. Yahiro et al. [19] stated that the bonding strength is not reduced in the case where the thickness of a diffusion layer is 3–5 μm, but it is deteriorated where the thickness increases to 10 μm or more and then making the clad sheet ineffective. Therefore, a sound interfacial bonded Mg/Al laminate is successfully fabricated by the proposed composite extrusion directly from the as-cast alloys. The EDS line analysis across the Mg/Al interface is plotted in Fig. 4. It reflects that, in the transition layer, the concentration of Al is decreased gradually from Al matrix to Mg matrix, while the Mg concentration presents an opposite tendency. The above phenomenon is in concordance with the research of Chen et al. [20], which implied that 6063 Al and AZ91 Mg alloys materials were miscible and the intermetallic was not formed in the interface of Mg/Al composite laminate fabricated by porthole die extrusion.

3.3. Microstructure characteristic of Mg alloy AZ31 layer of three extruded sheets

Fig. 5 presents the optical micrographs in the ED-ND plane of AZ31 layer of three extruded sheets. The conventional AZ31 sheet is characterized by an inhomogeneous microstructure with fine dynamic recrystallized grains embedding in a

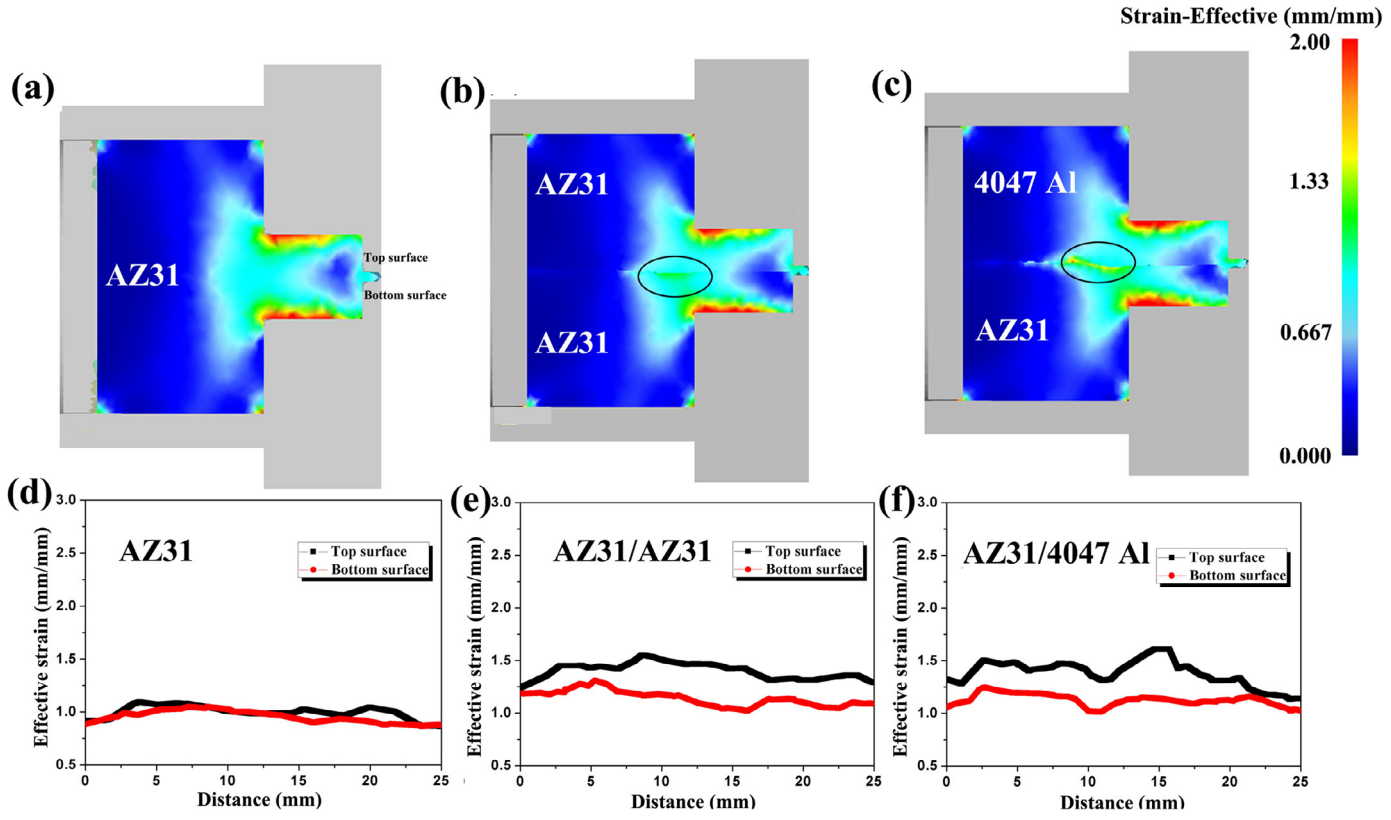

Fig. 3. The distribution of effective strain and effective strain evolution of top and bottom surfaces during extrusion processes: (a, d) conventional extruded AZ31 sheet. (b, e) composite extruded AZ31/AZ31 sheet. (c, f) composite extruded AZ31/4047 Al sheet.

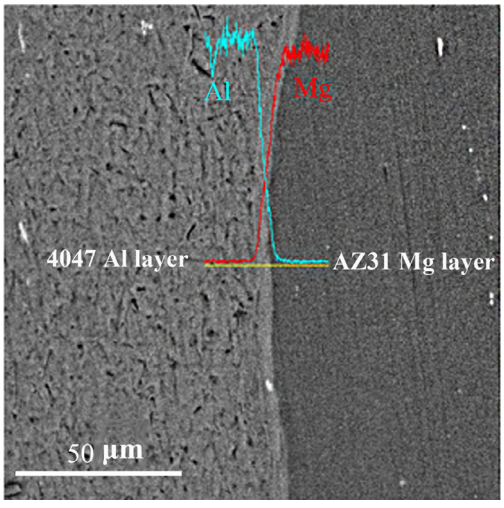

Fig. 4. SEM image of inter-diffusion reaction layers of AZ31/4047 Al composite extruded sheet.

relatively large region of elongated deformed grains, and its average grain size is ~10.3 μm (geometric standard deviation, $\sigma = 3.2$). In contrast, the AZ31/AZ31 sheet has a relatively higher microstructural homogeneity and smaller average grain size of ~9.4 μm ($\sigma = 2.0$). Besides, it is worth noting that obvious grain refinement (~5.6 μm, $\sigma = 0.9$) occurs in AZ31 layer of the AZ31/4047 Al sheet. The possible reason may be explained by as follows: (1) Strong sense of mixing and shearing force exists at the interface of two materials (see Fig. 3). The additional internal stress, especially the shear stress, can effectively refine the microstructure of Mg alloys during hot extrusion [21,22]. (2) Larger effective strain can be introduced during the process of hot co-extrusion, which is beneficial to acquire a homogeneous and fine microstructure eventually. (3) Owing to a higher thermal conductivity of Al alloy layer, the adiabatic heating localized near the interface during extrusion is mainly conducted by the Al alloy section and then contributes to the grain refinement of Mg layer [23,24].

The (0002) pole figures obtained in AZ31 layer from the AZ31, AZ31/AZ31 and AZ31/4047 Al sheets by XRD measurements are shown in Fig. 6. Compared with the AZ31 sheet with a typical basal texture in which the basal poles concentrating in the center of (0002) pole figure, a double-peak texture appears in the AZ31 layer of the AZ31/AZ31 sheet and its basal pole has an inclination of ~3° from the ND to the ED. The *c*-axis of most grains in the AZ31 layer of AZ31/4047 Al sheet is not collinear with the ND, rather, they are tilted towards the ED by approximately 6–7°. Apparently, the above phenomenon is essentially attributed to the introduced interface and different flow behaviors between AZ31 and 4047 Al alloys during the composite extrusion process. According to Fig. 3, it can be observed that more intense effective strain (at the interface) and strain gradient (throughout

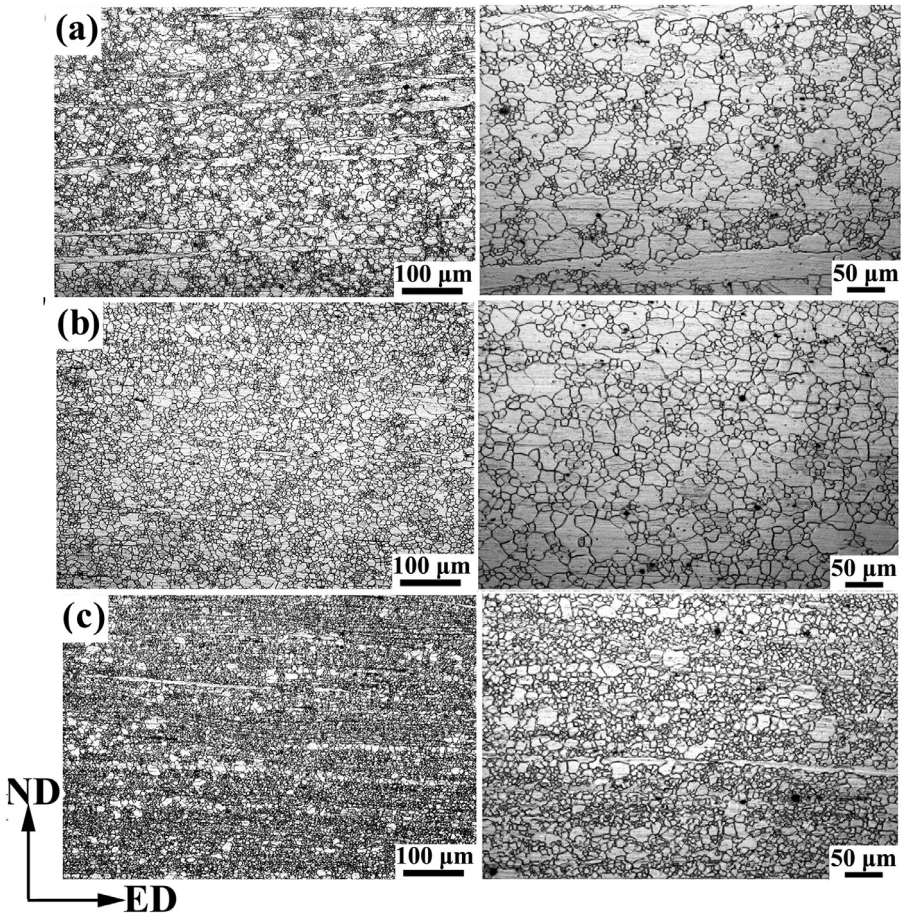

Fig. 5. Optical microstructures of Mg alloy AZ31 layer of three extruded sheets: (a) the AZ31 sheet. (b) The AZ31/AZ31 sheet. (c) The AZ31/4047 Al sheet.

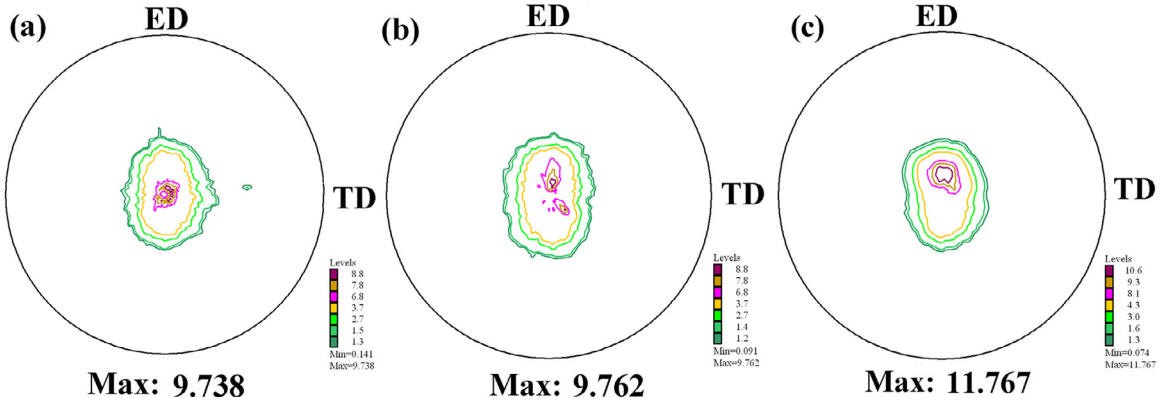

Fig. 6. (0002) pole figures obtained in AZ31 layer from three extruded sheets: (a) the AZ31 sheet. (b) The AZ31/AZ31 sheet. (c) The AZ31/4047 Al sheet.

the thickness direction) are introduced during the composite extrusion process of AZ31/AZ31 and AZ31/4047 Al sheets. So not only strong normal pressure stress caused by the extrusion mold (which can cause intense *c*-axis‖ND and lead to a strong basal texture), but also an additional mixing and shearing stress existing at the interface would in favor of the thermal plastic deformation during the composite extrusion. Related internal shear strain may influence the orientation of the recrystallized new grains by rotating the *c*-axis to some extent [25], thus producing tilted basal texture.

3.4. Tensile and compressive tests

Fig. 7(a) depicts the true tensile (*T*) and compressive (*C*) stress–strain curves of AZ31, AZ31/AZ31 and AZ31/4047 Al sheets. Fig. 7(b) presents the stress-strain curves of the total AZ31/4047 Al sheet and the monolayer AZ31 and 4047 Al sheets under uniaxial tensile and compressive tests. Yield strengths derived from Fig. 7 and the ratio between compressive yield strength and tensile yield strength (C/T) are given in Table 2. It is obvious that there is a

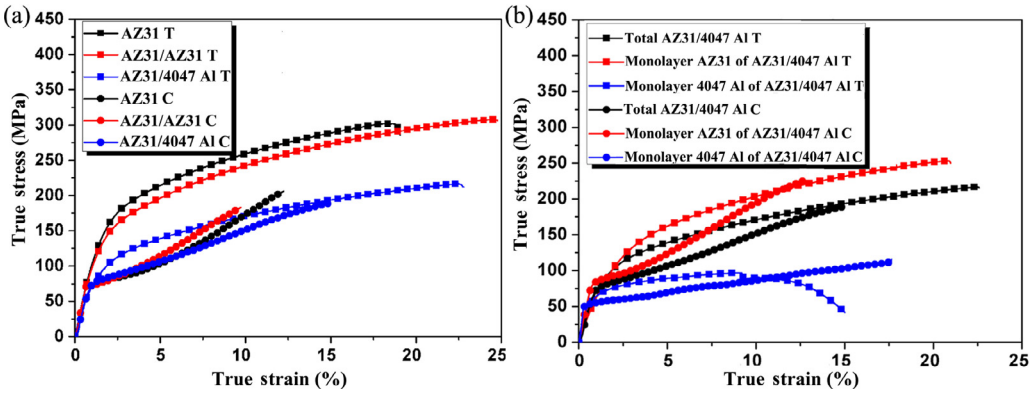

Fig. 7. (a) The true tensile (*T*) and compressive (*C*) stress–strain curves of three extruded sheets. (b) The true tensile (*T*) and compressive (*C*) stress–strain curves of the total AZ31/4047 Al sheet and the monolayer AZ31 and 4047 Al sheets.

Table 2
The summary of yield strength (YS) of several sheets which suffer from tensile and compressive tests, besides the ratio of compressive yield stress to the tensile yield stress (*C*/*T*) is also calculated.

Specimen	TYS (MPa)	CYS (MPa)	*C*/*T*
AZ31	141.5	82.2	0.58
AZ31/AZ31	130.8	78.6	0.61
AZ31/4047 Al	92.3	69.3	0.75
4047 Al	60.9	47.2	0.77

decreasing trend for tensile, compressive yield strengths and tension-compression yield asymmetry (TCA) from AZ31 to AZ31/AZ31 and AZ31/4047 Al sheets. Particularly, the C/T value of AZ31/4047 Al sheet reaches up to 0.75, much higher than that of AZ31 (0.58) and AZ31/AZ31 (0.61) sheets.

For the conventional extruded AZ31 sheet with a typical basal texture, its significant TCA was originated from the combinations of deformation twining polarity and different activated stress between deformation twinning and slip systems [9,26]. Correspondingly, extensive investigations have been devoted to reduce TCA by restraining {10–12} twins via grain refinement or texture modification [27] and so on. Dogan et al. [28] argued that grain size dependence of tensile twinning mode was more pronounced than that of dislocation slip. Hence, the reduced tension–compression yield asymmetry in the current work can be partly pertained to the twin suppressing induced by grain refinement. Besides, a tilted basal texture could not only facilitate the activity of basal slip under tension loading, but also delay twining activity during the compression process [29]. As a result, the slightly larger value of C/T in AZ31/AZ31 sheet compared to that of AZ31 sheet is assigned to the synergistic effects of refined grains and titled texture. Furthermore, the C/T value of AZ31/4047 Al composite sheet (0.75) in Table 2 is significantly higher than that of AZ31/AZ31 sheet (0.61). Hence, except for grain refinement and tilted texture in AZ31 layer (caused by the varied stress and strain states during composite extrusion via introduced Mg/Mg or Mg/Al interface), the existence of 4047 Al layer also contributes to the reduction of TCA in AZ31/4047 Al sheet. The possible reason is related to the high crystal symmetry of Al alloys (face-centred cubic structure, fcc) with abundant operable slip systems in tension and compression.

Fig. 8 presents the curves of strain hardening rate $\theta = (\partial\sigma/\partial\varepsilon)$ versus true stress after yielding of three extruded sheets in the tensile and compressive tests, where σ and ε are the true stress and true strain of the alloys, respectively. As showed in Fig. 8(a), the strain hardening rate of three sheets in tension all displays a monotonic decreasing trend, and the hardening extrapolation (θIII0) is gradually decreased from the AZ31 sheet to the AZ31/AZ31 and AZ31/4047 Al sheets. Del Valle et al. [30] stated that work hardening behavior was closely associated with the blocks and tangles of dislocations, which in turn reflected the magnitude of flow stress. Hence, the above phenomenon manifests that strength of AZ31/4047 Al sheet is lower than the corresponding value of AZ31 sheet in a tensile test. Besides, the curve slope of stage III (linear reduction stage) for three sheets in Fig. 8(a) are identical, which implies that their similar dynamic recovery ability in tension. When deformation was dominated by {10–12} twinning, the strain hardening rate could be divided into three distinct stages. Stage I was characterized by a falling strain hardening rate, followed by stage II with an inflection rising trend, again, there was a falling (stage III) [31]. Stage II is germane to the twinning activity. Once the twins are formed, twin boundaries will act as barriers for dislocation slip and then become a source of work hardening [32]. Hence, the length of stage II is predominantly related to the volume fraction of grains which are favorable for {10–12} twining [33]. It is worth noting that both the AZ31 and AZ31/AZ31 sheets have an inflection rising plateau in Fig. 8(b). The emergence of inflection rising plateau means that the main deformation mechanism has transformed the slip to twining. As for the composite extruded AZ31/4047 Al sheet, its essentially absent of inflection rising plateau in strain hardening rate curve can be attributed to the following two aspects: (1) Refined grains and tilted texture of Mg alloy AZ31 layer in composite AZ31/4047 Al sheet will restrict the formation of twins. (2) The 4047 Al layer also plays a critical role in the variation of strain hardening behavior. Coincidently, Feng et al. [12] also expressed that when the proportion of Al alloy layer

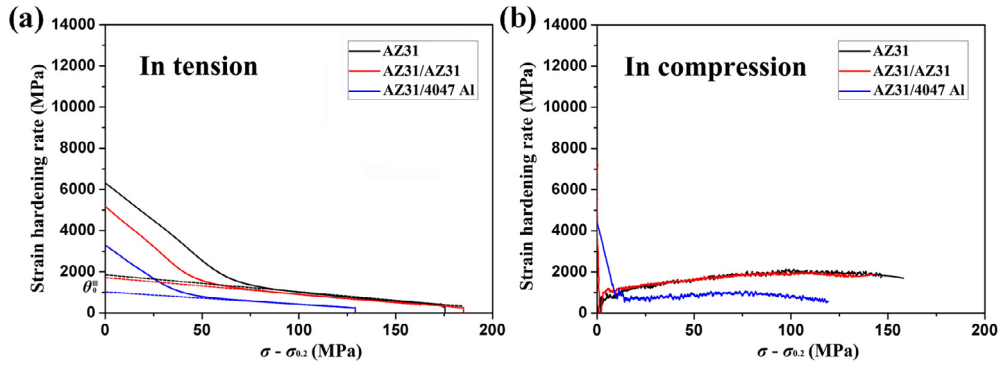

Fig. 8. The strain hardening rate curves of three extruded sheets: (a) in tension. (b) In compression.

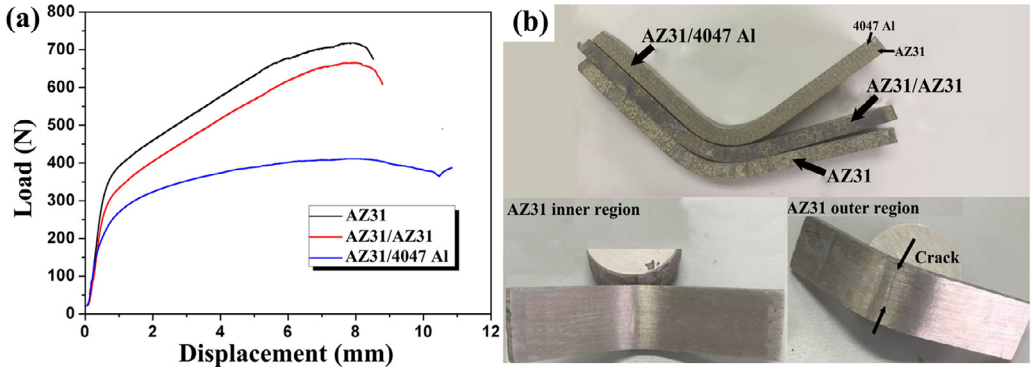

Fig. 9. (a) Load–displacement curves of three sheets under the same bending parameters at room temperature. (b) Appearance of the three sheets after bending forming and the specific location of crack initiation in AZ31 sheet during bending forming.

was large, the work hardening behavior of the whole Mg/Al sheet will be more prone to the characteristic of Al alloy.

3.5. The bending performance

Fig. 9(a) illustrates the load–displacement curves of three sheets under the same bending parameters at room temperature. As for curves of AZ31 and AZ31/AZ31 sheets, when the displacement is around 8 mm, the load decreases with the further increase of displacement (i.e., crack initiation and resulting stress release). In contrast, no fracture cracks are observed during the overall 90° bending process of extruded AZ31/4047 Al composite sheet, which indicates that it has a much better bendability than that of other two sheets. Fig. 9(b) depicts the appearance of three sheets after bending forming and the specific location of crack initiation in AZ31 sheet during bending forming. For the sake of simplicity, the condition of crack initiation in AZ31/AZ31 sheet is not repeated, owing to the similar situation between AZ31 and AZ31/AZ31 sheets. As a result, it can be observed that the cracks of AZ31 and AZ31/AZ31 sheets are initiated on the surface of the outer tensile region, while the counterparts of the inner compressive region are absent. Firstly, the phenomenon that cracks initiate at the edge region is related to the heterogeneous distributed stress and strain during the bending process. Jin et al. [34] reported that a strain gradient existed along the thickness direction of the sheet during bending forming via a commercial finite element (FEM). With more details, the maximum stress and strain were distributed in the inner or outer edge of the bending deformation region. Moreover, it is generally accepted that during bending of a sheet, the outer region is strained under tensile mode, whereas the inner region undergoes compressive deformation. Thus, when the tensile loading axis is parallel to the basal plane in the outer tensile region, twinning is not admissible, basal slip is also restricted, and only the prismatic ⟨a⟩ slip can coordinate the main deformation in the outer tensile region. However, slip direction of prismatic ⟨a⟩ is parallel to the basal plane and perpendicular to the direction of *c*-axis, which is unable to effectively coordinate the strain along the *c*-axis. As a result, due to the lack of coordination of the strain in the thickness direction, cracks on the surface of the outer tensile region initiate. In contrast, the existence of the {10–12} twins in the inner compressive region can effectively release the crack tip stress and eventually suppress the crack propagation [35,36], which is accountable for the fact that no significant cracks distribute in the inner compressive region.

As for AZ31/4047 Al composite sheet, the much better bendability can be summed up into several factors: (1) a tilted texture, basal poles tilted by about 6–7° away from the ND toward the ED, exists in the AZ31 layer of AZ31/4047 Al sheet. In this case, basal slip can be readily activated and then contributes to the improvement of thickness-direction strain accommodative ability in the outer tensile region. Aslam et al.

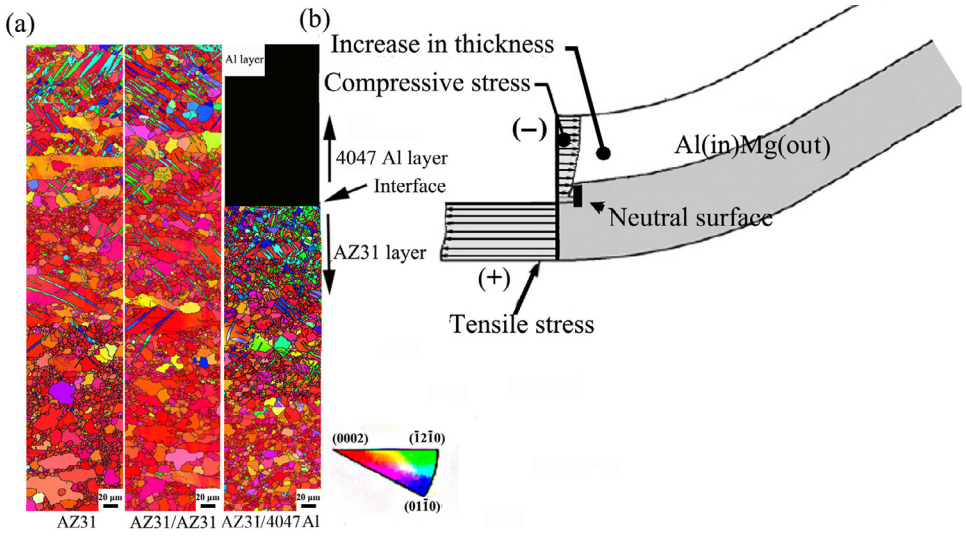

Fig. 10. (a) The EBSD inverse pole figure maps of Mg alloy AZ31 layer near the center of three bended samples. (b) Schematic illustration of the mechanism of sheet thickness variation.

[37] also declared that the excellent bendability of ZEK100 alloy was originated from the addition of rare earth elements inducing weakened and tilted basal texture. (2) In general, refined grains are in favor of the dislocation slip and strain coordination between grains during plastic deformation [38–41]. Hence, obvious grain refinement in the AZ31 layer of the AZ31/4047 Al sheet is beneficial to the deformability advancement of the outer tensile region. Besides, the low area fraction of elongated grains and the relative regular microstructures are in agreement with the better deformation compatibility. Similarly, Huang et al. [42] stated that the more homogenous microstructure, which was achieved by differential speed rolling, would contribute to the much higher ductility for the AZ80 alloy sheet. (3) The role of the 4047 Al layer cannot be ignored. Coincidently, Tokunaga et al. [43] concluded that, due to the interaction effect (suppression of necking) between Mg and Al layers, Al-coated Mg alloy sheet presents a superplastic behavior during low strain rate hot deformation.

3.6. The offset degree of bending strain neutral layer and sheet thickening

According to a theory of stamping process manual [44], the computational formula of the *k*-value (bending neutral layer coefficient) is shown as follows:

$$n = t_1/t \tag{1}$$

$$k = 0.5n^2 - (1-n)r/t \tag{2}$$

Where n is the thicken coefficient, t_1 is the thickness of sheet metal after bending, t is the original sheet thickness and r is the inside radius size of sample after bending. In general, *k*-value can be used to quantitatively evaluate the deviation between strain neutral layer and geometric neutral layer after bending forming. When *k*-value is 0.5, the strain neutral layer coincides with the geometric neutral layer. Besides, strain neutral layer shifts to the outer tensile region in the case of *k*-value greater than 0.5 and vice versa. In order to enhance the comparability of data, the sheet thickness variation and the *k*-value of three sheets are described under the circumstances that bending test is interrupted at 6 mm of punch displacement. The relative result is shown in Table 3.

Table 3
The list of thickness (include initial and bended state) and calculated *k*-value for AZ31, AZ31/AZ31 and AZ31/4047 Al sheets.

Specimen	Thickness [mm] (Initial)	Thickness [mm] (Punch displacement is 6 mm)	*k*-value
AZ31	2.51	2.54	0.58
AZ31/AZ31	2.47	2.48	0.56
AZ31/4047 Al	2.51	2.57	0.63

Generally speaking, the initial tension-compression yield asymmetry (TCA) degree of sheet can effectively reflect the variation of *k*-value in the subsequent bending forming. According to Tables 2 and 3, the C/T value is increasing from the AZ31 sheet to the AZ31/AZ31 sheet, while the *k*-value shows a downward trend instead. Similarly, Wang et al. [45] also expressed that the *k*-value of AZ31B alloys decreased as a result of the weakened TCA performance. However, it is worth mentioning that an abnormal phenomenon is appeared, wherein both the C/T value and *k*-value of AZ31/4047 Al sheet are larger than the corresponding values of AZ31 sheet. In fact, the C/T value of composite AZ31/4047 Al sheet in Table 2 is obtained via uniaxial tensile and compressive tests for the total sheet, while *k*-value in Table 3 reflects the difference between the inner compressive region (4047 Al layer) and outer tensile region (AZ31 layer) during bending forming. Hence, it is rational to speculate that C/T value (TCA performance) is not suitable to reflect the subsequent variation of *k*-value (the offset of bending strain neutral layer)

in composite AZ31/4047 Al sheet during bending forming. Fig. 10(a) illustrates the EBSD maps of Mg alloy AZ31 layer near the center of three bended samples. Apparently, the strain neutral layer of composite AZ31/4047 Al sheet has moved to the outer tensile region (AZ31 layer) after bending forming and this outward offset degree is much greater than that of AZ31 and AZ31/AZ31 sheets. The possible reason is ascribed to the quite wide gap of material properties between Mg alloy AZ31 layer (tensile loading in the outer region) and Al 4047 layer (compressive loading in the inner region). Yilamu et al. [46] also stated that when a clad sheet metal consisting of strong and weak layer was bent, the strain neutral surface would lie in the strong layer. Fig. 10(b) schematic elaborates the mechanism of sheet thickness variation during the bending forming process. As the outward migration of strain neutral layer, distribution of the stress state along the thickness direction of sheet changes correspondingly, in which the range of compressive stress expands and eventually crosses the geometry neutral layer, leading to the sheet thickening. Hence, it is revealed that the thickness increase of the AZ31/4047 Al sheet in Table 3 is affinitive with the phenomenon that the offset of its strain neutral layer to the outer tensile region.

4. Conclusions

1. A sound interfacial bonded AZ31/4047 Al sheet was successfully prepared via composite extrusion process. Compared with the conventional extruded AZ31 sheet (coarse grains and basal texture), refined grains and tilted texture in the AZ31 layer of AZ31/4047 Al sheet was mainly ascribed to the introduced interface and different flow behaviors between AZ31 and 4047 Al alloys during the composite extrusion process.
2. The tension-compression yield asymmetry presented a descend trend from the AZ31 to the AZ31/AZ31 and AZ31/4047 Al sheets. As for the room temperature bendability, the AZ31/4047 Al sheet could successfully accomplish the whole bending forming process, while the AZ31 and AZ31/AZ31 sheets were both bend-formed to failure. The bendability improvement of AZ31/4047 Al sheet was ascribed to 4047 Al laminate superposition and deformability advancement of the outer tensile region (AZ31 layer) via grain refinement and texture tilting.
3. Under the same bending strain, both outward offset degree of strain neutral layer and sheet thickening were more serious in the AZ31/4047 Al composite sheet than those of the AZ31 and AZ31/AZ31 sheets. The foremost reason was the quite wide gap of material properties between Mg alloy AZ31 layer (tensile loading in the outer region) and Al 4047 layer (compressive loading in the inner region).

Conflict of interest

None.

Acknowledgments

The authors are grateful for the financial supports from the National Key Research and Development Program of China (2016YFB0301104 and 2016YFB0101700), Chongqing Science and Technology Commission (cstc2017zdcy-zdzxX0006, cstc2017jcyjAX0012, cstc2018jcyjAX0472), and National Natural Science Foundation of China (51531002 and U1764253), Chongqing Scientific & Technological Talents Program (KJXX2017002), China Postdoctoral Science Foundation (2018T110948), Science and Technology Research Program of Chongqing Municipal Education Commission (KJQN201801306).

References

[1] B.L. Mordike, T. Ebert, Mater. Sci. Eng. A 302 (2001) 37–45.
[2] E. Dogan, M.W. Vaughan, S.J. Wang, I. Karaman, G. Proust, Acta Mater. 89 (2015) 408–422.
[3] T. Mukai, M. Yamanoi, H. Watanabe, K. Higashi, Scripta Mater. 45 (2001) 89–94.
[4] K.K. Alaneme, E.A. Okotete, J. Magn. Alloys 5 (2017) 460–475.
[5] E. Karakulak, J. Magn. Alloys 7 (2019) 355–369.
[6] S.H. You, Y.D. Huang, K.U. Kainer, N. Hort, J. Magn. Alloys 5 (2017) 239–253.
[7] D. Wu, R.S. Chen, E.H. Han, J. Alloys Compd. 509 (2011) 2856–2863.
[8] T.C. Xu, Y. Yang, X.D. Peng, J.F. Song, F.S. Pan, J. Magnes. Alloys 7 (2019) 536–544.
[9] S.W. Xu, K. Oh-Ishi, H. Sunohara, S. Kamado, Mater. Sci. Eng. A 558 (2012) 356–365.
[10] L.F. Wang, G.S. Huang, H. Zhang, Y.X. Wang, L. Yin, J. Mater. Process. Tech. 213 (2013) 844–850.
[11] J.K. Kim, T.X. Yu, J. Mater. Process. Tech. 63 (1997) 33–42.
[12] B. Feng, Y.C. Xin, F.L. Guo, H.H. Yu, Y. Wu, Q. Liu, Acta Mater. 120 (2016) 379–390.
[13] Y. Wu, B. Feng, Y.C. Xin, R. Hong, H.H. Yu, Q. Liu, Mater. Sci. Eng. A 640 (2015) 454–459.
[14] H. Chang, M.Y. Zheng, W.M. Gan, K. Wu, E. Maawad, H.G. Brokmeier, Scr. Mater. 61 (2009) 717–720.
[15] J.H. Bae, A.K. Prasada Rao, K.H. Kim, N.J. Kim, Scripta Mater. 64 (2011) 836–839.
[16] J.B. Sun, X.Y. Song, T.M. Wang, Y.S. Yu, M. Sun, Z.Q. Cao, T.J. Li, Mater. Lett. 67 (2012) 21–23.
[17] F.S. Pan, Q.H. Wang, B. Jiang, J.J. He, Y.F. Chai, J. Xu, Mater. Sci. Eng. A 655 (2016) 339–345.
[18] Q.H. Wang, B. Jiang, Y.F. Chai, B. Liu, S.X. Ma, J. Xu, F.S. Pan, Mater. Sci. Eng. A 673 (2016) 606–615.
[19] A. Yahiro, T. Masui, T. Yoshida, D. Doi, Temper. Mater. Trans. Iron Steel Inst. Jpn. 31 (2007) 647–654.
[20] L. Chen, J.W. Tang, G.Q. Zhao, C.S. Zhang, X.R. Chu, J. Mater. Process. Tech. 258 (2018) 165–173.
[21] M. Negendank, S. Mueller, W. Reimers, J. Mater. Process. Tech. 212 (2012) 1954–1962.
[22] K. Osakada, M. Limb, P.B. Mellor, Int. J. Mech. Sci. 15 (1973) 291–307.
[23] J.C. Williams, E.A. Starke, Acta Mater. 51 (2003) 5775–5799.
[24] D.K. Yang, P. Cizek, P. Hodgson, C.E. Wen, Scripta Mater. 62 (2010) 321–324.
[25] Y. Chino, K. Kimura, M. Hakamada, M. Mabuchi, Mater. Sci. Eng. A 485 (2008) 311–317.
[26] D.L. Yin, J.T. Wang, J.Q. Liu, X. Zhao, J. Alloys Compd. 478 (2009) 789–795.
[27] S.M. Yin, C.H. Wang, Y.D. Diao, S.D. Wu, S.X. Li, J. Mater. Sci. Technol. 27 (2011) 29–34.

[28] E. Dogan, I. Karaman, G. Ayoub, G. Kridli, Mater. Sci. Eng. A 610 (2014) 220–227.
[29] L.F. Wang, E. Mostaed, X.Q. Cao, G.S. Huang, A. Fabrizi, F. Bonollo, C.Z. Chi, M. Vedani, Mater. Des. 89 (2016) 1–8.
[30] J.A. Del Valle, F. Carreño, O.A. Ruano, Acta Mater. 54 (2006) 4247–4259.
[31] S.G. Hong, S.H. Park, S.L. Chong, Acta Mater. 58 (2010) 5873–5885.
[32] N. Li, J. Wang, A. Misra, X. Zhang, J.Y. Huang, J.P. Hirth, Acta Mater. 59 (2011) 5989–5996.
[33] B.S. Wang, R.L. Xin, G.S. Huang, Q. Liu, Mater. Sci. Eng. A 534 (2012) 588–593.
[34] L. Jin, J. Dong, J. Sun, A.A. Luo, Int. J. Plastic. 72 (2015) 218–232.
[35] L. Wu, S.R. Agnew, D.W. Brown, G.M. Stoica, B. Clausen, A. Jain, D.E. Fielden, P.K. Liaw, ZK60A Acta Mater 56 (2008) 3699–3707.
[36] F.Y. Liu, C.F. Guo, R.L. Xin, G.L. Wu, Q. Liu, J. Magnes. Alloys 7 (2019) 258–263.
[37] I. Aslam, B. Li, Z. McClelland, S.J. Horstemeyer, Q. Ma, P.T. Wang, M.F. Horstemeyer, Mater. Sci. Eng. A 590 (2014) 168–173.
[38] H.X. Wang, L.X. Zhang, W.Z. Chen, D.Q. Fang, W.C. Zhang, G.R. Gui, Mater. Sci. Eng. A 736 (2018) 239–247.
[39] F. Abouhilou, A. Hanna, H. Azzeddine, D. Bradai, J. Magnes. Alloys 7 (2019) 124–133.
[40] Y.F. Chai, B. Jiang, J.F. Song, B. Liu, G.S. Huang, D.F. Zhang, F.S. Pan, Mater. Sci. Eng. A 746 (2019) 82–93.
[41] Y.F. Chai, B. Jiang, J.F. Song, Q.H. Wang, H. Gao, B. Liu, G.S. Huang, D.F. Zhang, F.S. Pan, J. Alloys Compd. 782 (2019) 1076–1086.
[42] X.S. Huang, K. Suzuki, N. Saito, Mater. Sci. Eng. A 508 (2009) 226–233.
[43] T. Tokunaga, K. Matsuura, M. Ohno, J. Alloys Compd. 601 (2014) 179–185.
[44] G.S. Huang, Y.X. Wang, L.F. Wang, T.Z. Han, F.S. Pan, Trans. Nonferrous Met. Soc. China 25 (2015) 732–737.
[45] L.F. Wang, G.S. Huang, F.S. Pan, M. Vedani, Mater. Lett. 143 (2015) 44–47.
[46] K. Yilamu, R. Hino, H. Hamasaki, F. Yoshida, Mater. Process. Tech. 210 (2010) 272–278.